

**Investigation of the crystal structure of low water content hydrous olivine to 29.9 GPa: a high-pressure single-crystal X-ray diffraction study**

**Jingui Xu<sup>1, 2</sup>, Dawei Fan<sup>1</sup>, Dongzhou Zhang<sup>2</sup>, Bo Li<sup>1, 3</sup>, Wenge Zhou<sup>1</sup> and Przemyslaw K. Dera<sup>2</sup>**

<sup>1</sup>Key Laboratory for High-Temperature and High-Pressure Study of the Earth's Interior, Institute of Geochemistry, Chinese Academy of Sciences, Guiyang 550081, China.

<sup>2</sup>Hawai'i Institute of Geophysics and Planetology, School of Ocean and Earth Science and Technology, University of Hawai'i at Manoa, Honolulu, Hawaii 96822, United States.

<sup>3</sup>University of Chinese Academy of Sciences, Beijing, 100049, China.

Corresponding author: Dawei Fan ([fandawei@vip.gyig.ac.cn](mailto:fandawei@vip.gyig.ac.cn))

## Abstract

Olivine is the most abundant mineral in the Earth's upper mantle and subducting slabs. Studying the structural evolution and equation of state of olivine at high-pressure is of fundamental importance in constraining the composition and structure of these regions. Hydrogen can be incorporated into olivine and significantly influence its physical and chemical properties. Previous infrared and Raman spectroscopic studies indicated that local structural changes occur in Mg-rich hydrous olivine ( $\text{Fo} \geq 95$ ; 4883-9000 ppmw water) at high-pressure. Water contents of natural olivine are commonly less than 1000 ppmw, it is thus inevitable to investigate the effects of such water contents on the equation of state (EoS) and structure of olivine at high-pressure. Here we synthesized low water content hydrous olivine ( $\text{Fo}_{95}$ ; 1538 ppmw water) at low  $\text{SiO}_2$  activity and identified that the incorporated hydrogens are predominantly associated with the Si sites. We performed high-pressure single-crystal X-ray diffraction experiments on this olivine to 29.9 GPa. A third-order Birch-Murnaghan equation of state (BM3 EoS) was fit to the pressure-volume data, yielding the following EoS parameters:  $V_{T0} = 290.182(1) \text{ \AA}^3$ ,  $K_{T0} = 130.8(9) \text{ GPa}$ , and  $K'_{T0} = 4.16(8)$ . The  $K_{T0}$  is consistent with those of anhydrous Mg-rich olivine, which indicates that such low water content has negligible effects on the bulk modulus of olivine. Furthermore, we carried out the structural refinement of this hydrous olivine as a function of pressure to 29.9 GPa. The results indicate that, similar to the anhydrous olivine, the compression of the M1-O and M2-O bonds are comparable, which are larger than that of the Si-O bonds. The compression of M1-O and M2-O bonds of this hydrous olivine are comparable with those of anhydrous olivine, while the Si-O1 and Si-O2 bonds in the hydrous olivine are more compressible than those in the anhydrous olivine. Therefore, this study suggests that low water

content has negligible effects on the EoS of olivine, though the incorporation of water softens the Si-O1 and Si-O2 bond.

## 1. Introduction

The incorporation of water into mantle nominally anhydrous minerals (NAMs) has been a hot topic of geophysics and geochemistry, as it strongly influences the physical and chemical properties of NAMs. Among the main mineral phases in the upper mantle, olivine is undoubtedly the center of the topic, due to its large abundance in the mantle (Ita and Stixrude 1992). Natural mantle-derived olivine can contain a few to hundreds of ppmw of water (e.g., Bell and Rossman 1992; Beran and Libowitzky 2006; Peslier 2010). Several factors affect the water solubility of olivine, including pressure, temperature, oxygen fugacity, water fugacity, and silica activity (e.g., Fei et al. 2018; Kohlstedt et al. 1996; Mosenfelder et al. 2006; Qin et al. 2018; Smyth et al. 2006). Experimental studies have suggested that the maximum is as high as 8900 ppmw (Smyth et al. 2006).

The incorporation of hydrogen in olivine and its effects on the various physical and chemical properties have long been investigated (e.g., Jacobsen et al. 2008; Mao et al. 2010; Chen et al. 2011; Ghosh et al. 2013; Manghnani et al. 2013; Wang et al. 2019). Vibrational spectroscopy (such as infrared spectroscopy) has been mostly employed to qualitatively and quantitatively determine the extent of incorporation of hydrogen. In a Fourier transform infrared spectroscopy (FTIR) spectrum, the O-H vibrational bands are within the region of 3000-3700 cm<sup>-1</sup>. However, the mechanisms of hydrogen incorporation, as constrained by the locations of these vibrational bands have long been controversial. The most significant controversy concerns which substitution mechanism accounts for the high-frequency O-H bands above 3450 cm<sup>-1</sup>. Some of

the previous studies have interpreted these bands in terms of the  $2\text{H}^+$  for  $\text{Mg}^{2+}$  substitution associated with the Mg vacancies, based on the polyhedral O-O edge lengths (e.g., Kudoh et al. 2006; Smyth et al. 2006; Hushur et al. 2009; Manghnani et al. 2013). However, other studies have attributed these bands to the  $4\text{H}^+$  for  $\text{Si}^{4+}$  substitution associated with the Si vacancies, based on the compositional effects on the incorporation of water (e.g., Matveev et al. 2001; Berry et al. 2005; Berry et al. 2007; Kovács et al. 2010).

Recently, combined nuclear magnetic resonance (NMR), vibrational spectroscopy and first-principles calculation studies have led to a conclusion that the high-frequency O-H bands above  $3450\text{ cm}^{-1}$  in olivine are due to the  $4\text{H}^+$  for  $\text{Si}^{4+}$  substitution associated with the Si vacancies, which is the predominant hydration mechanism in olivine, and the  $2\text{H}^+$  for  $\text{Mg}^{2+}$  substitution associated with the Mg vacancies is responsible for the low-frequency ( $< 3400\text{ cm}^{-1}$ ) O-H bands (e.g., Balan et al. 2011; Umemoto et al. 2011; Balan et al. 2017; Xue et al. 2017).

However, most of these studies on the hydrogen incorporation mechanism were performed at ambient conditions. Very recently, an in situ High-pressure FTIR study on hydrous olivine has revealed hydrogen transfer between the Si storage sites with pressure (Yang et al. 2019). Therefore, it is important to investigate the effects of the hydrogen transfer on the structure and equation of state (EoS) of olivine at high-pressure. However, compared to anhydrous olivine (Mao et al. 1970; Liu 1975; Durben et al. 1993; Liu and Mernagh 1993; Andrault et al. 1995; Downs et al. 1996; Zha et al. 1998; Zhang 1998; Rouquette et al. 2008; Nestola et al. 2011; Finkelstein et al. 2014; Zhang et al. 2017b; Angel et al. 2018; Zhang et al. 2019), high-pressure studies on hydrous olivine are relatively limited (e.g., Manghnani et al. 2013). At ambient temperature, high-pressure powder X-ray diffraction (PXRD) experiments revealed that olivine containing several thousand ppmw water retains its structure to  $\sim 34\text{ GPa}$ . However, high-

pressure Raman spectroscopy (RS) has detected subtle discontinuous changes around 20 GPa (Hushur et al. 2009; Manghnani et al. 2013).

Previous studies suggested that the incorporation of several thousand ppmw water ( $\geq 4883$  ppmw) has effects on the elasticity and EoS of olivine (e.g., Jacobsen et al. 2008; Hushur et al. 2009; Mao et al. 2010; Manghnani et al. 2013); however, the water contents of natural mantle olivine are commonly less than 1000 ppmw (e.g., Peslier 2010). Therefore, it is inevitable to investigate the effects of relatively low water content on the EoS and structure of olivine at high-pressure. High-pressure single-crystal X-ray diffraction (SCXRD) is a powerful tool for investigating the pressure-induced changes in the crystal structure and provides the most reliable unit-cell parameter data to determine the EoS (Angel et al. 2000; Dubrovinsky et al. 2010). With high-pressure SCXRD, one can determine the effects of pressure on the compression of the individual coordination polyhedron, and thus examine the effects of incorporation of hydrogen associated with cationic vacancies. As a result, SCXRD may be able to investigate the effects of minor water content on the olivine structure at high-pressure. Here we report a high-pressure SCXRD study to investigate the EoS and structural evolution of low water content hydrous Mg-rich olivine (Fo<sub>95</sub>; 1538 ppmw water). Furthermore, the effects of water on the EoS and high-pressure structure of olivine will be discussed.

## **2. Materials and Methods**

### **2.1. Synthesis of hydrous olivine**

The olivine used in this study was synthesized by the method of high-pressure solid-solid reactions using a multi-anvil pressure apparatus at the Institute of Geochemistry, Chinese Academy of Sciences, Guiyang, China. The sample assembly was similar to the authors'

previous study (Fan et al. 2017; Xu et al. 2018). To obtain hydrous olivine, we used an omphacite + brucite ( $\text{Mg}(\text{OH})_2$ ) mixture as the starting material. Several natural omphacite crystals with grain sizes of  $\sim 200\text{--}400\ \mu\text{m}$ , were selected from a crushed large eclogitic omphacite. The brucite powder was used as the water source surrounding omphacite crystals in the experimental platinum capsule. We used a Ni foil as the oxygen buffer in the synthesis (Rauch and Keppler 2002; Xu et al. 2018). This sample assembly allowed olivine to grow at low  $\text{SiO}_2$  activity. The sample was first compressed to 4.0 GPa over 35 minutes and then heated to  $1200\ ^\circ\text{C}$  in 30 minutes. After a run duration of 24 hours, the olivine crystals ( $100\text{--}400\ \mu\text{m}$  size) were obtained from the quenched run product.

## 2.2. Chemical and FTIR Analysis

Selected crystals with sizes larger than  $\sim 100\ \mu\text{m}$  were used for electron microprobe analysis (EMPA). Analyses were performed with a JEOL Hyperprobe JXA-8500F microscope, operating at a 15 kV accelerating voltage, 20 nA beam current, and the beam size of  $10\ \mu\text{m}$ . The empirical chemical formula was calculated as  $\text{Mg}_{1.904\pm 9}\text{Ni}_{0.089\pm 9}\text{Fe}_{0.015\pm 3}\text{Si}_{0.991\pm 1}\text{O}_4$  based on the EMPA data (Table S1). The composition of the sample expressed in end-member molar percentages is  $\text{Fo}_{95}\text{Lie}_5$ , where Fo and Lie are forsterite ( $\text{Mg}_2\text{SiO}_4$ ) and liebenbergite ( $\text{Ni}_2\text{SiO}_4$ ), respectively. Unpolarized FTIR was employed to analyze the incorporation of water in the olivine. We obtained two crystals without any inclusions or fractures from the quenched products for the FTIR analysis, and the grain size was  $\sim 400\ \mu\text{m}$ . The experimental details can be seen in Xu et al. (2018). The obtained FTIR spectra (Figure 1) were very similar to previous studies on synthetic olivine (Lemaire et al. 2004; Smyth et al. 2006) and indicated that the sample has four strong peaks at  $3612$ ,  $3577$ ,  $3565$  and  $3555\ \text{cm}^{-1}$ , and a weaker peak at  $3477\ \text{cm}^{-1}$ . These peaks are

associated with the Si site (Kohlstedt et al. 1996; Lemaire et al. 2004; Berry et al. 2005; Berry et al. 2007; Walker et al. 2007; Xue et al. 2017). Additionally, a broad peak located between 3100 and 3400  $\text{cm}^{-1}$  confirmed that the  $2\text{H}^+$  for  $\text{Mg}^{2+}$  substitution also takes place in the synthetic olivine, but its extent is rather insignificant, relative to that at Si sites (Lemaire et al. 2004; Xue et al. 2017). The water content was estimated from integrated absorbances using the calibration of Bell et al. (2003), and the result was 1538(37) ppmw.

### 2.3. Single-crystal X-ray diffraction at high-pressure

An olivine crystal with size ca.  $40 \times 35 \times 7 \mu\text{m}$  was selected from the crushed FTIR sample, which was mounted onto a polymer holder for ambient SCXRD measurement. Then, the same sample was loaded into a short symmetric diamond anvil cell (DAC) with two Type-I diamonds (300  $\mu\text{m}$  culets) mounted on Boehler-Almax-type WC seats, and this sample assembly allowed a  $\pm 32^\circ$  opening angle. A rhenium gasket was indented to a thickness of  $\sim 40 \mu\text{m}$  by the diamond anvils, and a 180- $\mu\text{m}$  sample chamber was cut using a laser drilling following indentation. Gold powder was loaded as pressure marker (Fei et al. 2007). A small ruby sphere was loaded as the pressure indicator for the gas-loading with neon (Rivers et al. 2008).

Ambient and high-pressure SCXRD experiments were carried out with a six-circle diffractometer at the experimental station 13-BM-C of the Advanced Photon Source, Argonne National Laboratory. The experimental details can be seen in previous studies (e.g., Xu et al. 2017a; Zhang et al. 2017a). To obtain precise and sufficient data to constrain the unit-cell evolution with pressure, we collected the diffraction data at 40 different pressures over 0-29.9 GPa (Table S2), and at least 150 reflections (Figure 2) were used to refine the unit-cell parameters at each pressure point. In addition, we collected diffraction data with increased

coverage/more reflections (at least 550) with multiple detector positions at 11 different pressures for full structure determination (Table S3). The refinement of the unit-cell parameters and the data reduction were completed with the GSE\_ADA/RSV software package (Dera et al. 2013). Structure refinements at various pressures were carried out with SHELXL, Olex2, and VESTA software packages (Sheldrick 2008; Dolomanov et al. 2009; Momma and Izumi 2011). We employed a previously reported olivine structure (Nord et al. 1982) as the initial model of the structure refinement. In the olivine structure (M1M2TO<sub>4</sub>), there are two non-equivalent octahedral sites M1 and M2. In the ambient structural refinement, the T sites were fully occupied by Si, while the M1 and M2 sites are fully occupied by a mixture of Mg and Ni with a refinable ratio. We did not include Fe in the refinement as it has a similar electron number with Ni and its insignificant content compared to Mg and Ni. Atoms sharing the same site were set to share the same fractional coordinates and atomic displacement parameters (ADP). Anisotropic ADP was applied to all atoms. Ambient structure refinement led to the Mg/Ni ratios of 91/9 and 98/2 for M1 and M2, respectively, which was very consistent with the results of the chemical analysis. In the high-pressure structural refinements, the Mg/Ni ratios of M1 and M2 were fixed at 91/9 and 98/2, respectively, and isotropic ADP was applied to all atoms, due to the limited opening angle of the DAC. Unit-cell parameters, refinement details, atomic coordinates, as well as calculated polyhedral parameters including bond length and volume are listed in Tables S(2-6). The cif files can be obtained in the supplementary material.

### **3. Results and discussion**

#### **3.1. Equation of state and compressional behavior of coordination polyhedral geometry**



Upon compression, olivine retained its initial structure to the maximum pressure of 29.9(2) GPa. The unit-cell parameters of olivine decreased continuously with increasing pressure over the experimental range of 0-29.9 GPa, as shown in Figure 3. The pressure-volume ( $P$ - $V$ ) data were fit without any constraints, using a third-order Birch-Murnaghan (BM3) EoS (Birch 1947) using the program EoSFit7c (Angel et al. 2014; Gonzalez-Platas et al. 2016). The obtained EoS parameters including zero- $P$  unit-cell volume ( $V_0$ ), isothermal bulk modulus ( $K_{T0}$ ), and its pressure derivative ( $K'_{T0}$ ) were  $V_0 = 290.182(1) \text{ \AA}^3$ ,  $K_{T0} = 130.8(9) \text{ GPa}$ , and  $K'_{T0} = 4.16(8)$ , respectively. We also determined the EoS for each unit-cell edge using a BM3 EoS. The results are reported in Table S7, which shows that the  $b$  direction is the softest, while  $a$  is the stiffest; the axial compressibility scheme is  $\beta_b > \beta_c > \beta_a$ . The  $F_E$ - $f_E$  plot (Birch 1978; Angel 2000) is shown in Figure 4, which shows that data for  $a$ ,  $b$ ,  $c$ , and  $V$  lie on inclined straight lines, and a weighted linear fit of the  $F_E$ - $f_E$  data yielded  $K_{T0}$  and  $K'_{T0}$ , which are in excellent agreement with those indicated by the BM3 EoS fit (Table S7), indicating that the BM3 EoS is a reasonable choice to fit the high-pressure data.

To better understand the compression mechanism, we analyzed the polyhedral evolution with pressure using the structure refinements at high-pressure. As in previous high-pressure studies on olivine and other mantle major minerals such as pyroxene (Zhang et al. 1997; Periotto et al. 2012; Xu et al. 2017b), in the hydrous olivine, the  $\text{SiO}_4$  tetrahedron was much more incompressible than the  $\text{M1O}_6$  and  $\text{M2O}_6$  octahedra (Figure 5). As shown in Figure 5, polyhedral volumes of  $\text{M1O}_6$  and  $\text{M2O}_6$  underwent nearly linear compression, accompanying the decrease of the unit-cell volume.  $\text{M2O}_6$  is slightly more compressible than  $\text{M1O}_6$ . The  $\text{SiO}_4$  tetrahedron is much stiffer than  $\text{M1O}_6$  and  $\text{M2O}_6$ . The compressional behavior of the  $\text{M1O}_6$  and  $\text{M2O}_6$  is very close to that of the unit-cell volume (Figure 5), thus control the bulk compression of the olivine

structure. The bond lengths of M1-O, M2-O, and Si-O as a function of pressure are shown in Figures (6-8). During compression from 0 to 29.9 GPa, the mean bond length of M1-O and M2-O shortened by 5 and 7%, respectively. By comparison, the Si-O bonds were much stiffer, only shortened by 2% over the experimental pressure range.

### 3.2. Effects of water on compression behavior of olivine

We compared the EoS results of the hydrous olivine in this study to those of Mg-rich (Fo  $\geq$  95) olivine from previous studies. To make the comparison reasonable, only the data collected using high-pressure SCXRD from the previous studies were considered. The EoS determination of Hazen (1976) was based on only four pressure measurements to a maximum pressure of 5 GPa, and such data coverage should be insufficient to allow robust refinements of three EoS parameters ( $V_{T0}$ ,  $K_{T0}$ , and  $K'_{T0}$ ), thus we did not consider it. The EoS study of Kudoh and Takéuchi (1985) was based on 7 pressure measurements within 3.1-14.9 GPa, as they used a 4:1 mixture of methanol and ethanol as the pressure medium, and only five data (3.1-8.6 GPa) were collected under hydrostatic conditions (Angel et al. 2007). Therefore, for the same reason mentioned above, we did not consider the EoS results of Kudoh and Takéuchi (1985) as well. Finally, the EoS parameters of anhydrous Fo<sub>100</sub> obtained by Downs et al. (1996), Zhang (1998), Poe et al. (2010) and Finkelstein et al. (2014) were considered. Due to the effects of the trade-off between the  $K_{T0}$  and  $K'_{T0}$ , we refitted the  $P$ - $V$  data of the previous studies (Downs et al. 1996; Zhang 1998; Poe et al. 2010; Finkelstein et al. 2014) and this study with fixed  $K'_{T0} = 4.2$  that is the value for the anhydrous Fo<sub>100</sub> suggested by a high-pressure Brillouin Light Scattering study (Zha et al. 1996). By doing so, the fitting of the  $P$ - $V$  data of the previous studies obtained  $K_{T0}$  of 124(3)-130.4(4) GPa, which are comparable to the  $K_{T0}$  derived from the fitting of the  $P$ - $V$  data in this study (130.5(2) GPa). Therefore, low water content (1538 ppmw) could have negligible

effects on the  $K_{70}$  of olivine. However, previous studies on hydrous olivine with water contents larger than or equal to 4883 ppmw suggested that such water contents reduce the bulk modulus of olivine (Jacobsen et al. 2008; Mao et al. 2010; Manghnani et al. 2013).

We also compared the compressions of bond lengths and polyhedral volumes of hydrous olivine in this study to those of anhydrous olivine from previous studies. As shown in Figures (6-9), the hydrous olivine Fo<sub>95</sub> in this study and anhydrous Fo<sub>100</sub> from Pamato et al. (2019) are in good agreement in the compression trends of M1-O, M2-O, and Si-O bonds. However, the compressions of bond lengths of anhydrous Fo<sub>100</sub> from earlier high-pressure SCXRD studies (Hazen 1976; Kudoh and Takéuchi 1985) deviate the trends determined by this study and Pamato et al. (2019), which is possibly caused by the lower accuracy of diffractometers decades ago, as indicated by the larger uncertainties of the unit-cell parameters and bond lengths (Figures 3 and (6-8)). Therefore, we only further compared our results of the bond lengths to those of anhydrous Fo<sub>100</sub> from Pamato et al. (2019).

We analyzed the pressure-bond length and pressure-polyhedral volume data of olivine in this study and Pamato et al. (2019) by using weighted linear regression (Figures (6-9) and Table S8). Due to the data range of Pamato et al. (2019) was 0-7.66 GPa, only the data within the range of 0-10 GPa of this study were used, to make the comparisons reasonable. As shown in Figures (6-7) and Table S8, the compressions of M1-O and M2-O between the anhydrous and hydrous olivine are similar. The M1-O bonds of the anhydrous Fo<sub>100</sub> decrease near linearly with pressure and the rates are 0.0044(3)-0.0054(2) Å/GPa, which are comparable with the shrinking rates of the M1-O bonds for the hydrous Fo<sub>95</sub> (0.0036(3)-0.0048(2) Å/GPa; Figure 6). Similarly, the M2-O bonds of these two olivines decrease with pressure at comparable rates of 0.0049(5)-0.0077(6) and 0.0053(3)-0.0069(6) Å/GPa for the anhydrous Fo<sub>100</sub> and hydrous Fo<sub>95</sub> (Figure 7),

respectively. The similarity in the compressions of M1-O and M2-O bond lengths between the anhydrous and hydrous olivine results in the comparable polyhedral (M1O<sub>6</sub> and M2O<sub>6</sub>) compressibilities between the hydrous and anhydrous olivine (Figure 9).

Compared with M1-O and M2-O, the Si-O bonds behave quite differently under pressure between the anhydrous and hydrous olivine (Figure 8). As shown in Figure 8 and Table S8, for the anhydrous Fo<sub>100</sub>, the Si-O1 and Si-O2 bonds decrease at very low rates of 0.0006(7) and 0.0010(5) Å/GPa, respectively. Additionally, the small values of the correlation coefficients ( $R^2$  = 0.394 and 0.084 for the Si-O1 and Si-O2, respectively) indicate the variation of bond length is insensitive to the pressure change, while the compression of the Si-O3 is more significant as indicated by the higher shrinking rate (0.0015(1) Å/GPa) and  $R^2$  (0.936). The Si-O1 and Si-O2 bonds in the hydrous Fo<sub>95</sub> are more compressible than those in the anhydrous Fo<sub>100</sub>. As shown in Figure 8 and Table S8, the bond lengths of the Si-O1 and Si-O2 of hydrous Fo<sub>95</sub> decrease at rates of 0.0025(2) and 0.0013(6) Å/GPa, respectively, and the higher  $R^2$  values (0.992 and 0.731 for the Si-O1 and Si-O2, respectively) also indicate that the bond length is more sensitive to the pressure change than that of the anhydrous Fo<sub>100</sub>. On the other hand, the shrinking rate of the Si-O3 for the hydrous Fo<sub>95</sub> (0.0011(1) Å/GPa) is lower than that for the anhydrous Fo<sub>100</sub> (0.0015(1) Å/GPa). In a view of the polyhedral compression, the SiO<sub>4</sub> tetrahedron in the hydrous Fo<sub>95</sub> is more compressible than that in the anhydrous Fo<sub>100</sub> olivine (Figure 9).

#### 4. Implications

Previous high-pressure spectroscopic and XRD studies suggested that the incorporation of several thousand ppmw of water ( $\geq 4883$  ppmw) causes some local structural changes at high-pressure and affects the elasticity and EoS of olivine (e.g., Jacobsen et al. 2008; Hushur et al.

2009; Mao et al. 2010; Manghnani et al. 2013; Yang et al. 2019). However, the water contents of natural olivine are commonly less than 1000 ppmw (e.g., Peslier et al. 2010; Novella et al. 2015), and petrological experiments also suggested that the water storage capability of olivine in peridotite in the upper mantle is lower than 2000 ppmw (Ferot and Bolfan-Casanova 2012; Tenner et al. 2012). Therefore, the water contents of mantle olivine, in most cases, should be less than 2000 ppmw. In this study, the hydrous olivine was with moderate water content (1538 ppmw) that could be more expected in real mantle olivine than those in hydrous olivine from the previous studies. The EoS determination indicated that such low water content has negligible effects on the bulk modulus. In addition, the detailed structural refinements at high-pressure suggested that the compressions of the M1-O and M2-O bonds of the hydrous olivine in this study are similar to those of anhydrous olivine from the previous study. However, the compressions of the Si-O bonds were changed by the incorporation of water, and the Si-O1 and Si-O2 bond in the hydrous olivine are significantly more compressible than those in the anhydrous olivine. Our FTIR measurements indicated that the incorporation of hydrogen is predominantly associated with the vacancies in Si sites (Figure 1), which is consistent with the fact that the incorporation of water softens the Si-O bonds instead of the M1-O and M2-O bonds (Figures 6-9). However, the water-induced change in the compressional behavior of the Si-O bonds does not affect the bulk compression of olivine significantly. The incorporation of ~1500 ppmw does not significantly reduce the bulk modulus of olivine, which can be interpreted in terms of that such low water content has negligible effects on the compressional wave velocity, according to the Newton-Laplace equation approximation. Therefore, the results of this study indicate that the effects of incorporation of water on the elasticity and EoS of olivine could be significant only when the water content is at least higher than 1538 ppmw.

## 281 Acknowledgments

282 Sincere thanks go to Sergey N. Tkachev for help with gas loading. This project was  
283 funded by the National Natural Science Foundation of China (Grant Nos. 41772043, and  
284 41802043), the Chinese Academy of Sciences “Light of West China” Program (2017, 2019), the  
285 Youth Innovation Promotion Association CAS (Dawei Fan, 2018434), and the Innovation and  
286 Entrepreneurship Funding of High-Level Overseas Talents of Guizhou Province (Dawei Fan,  
287 [2019]10). Part of this work was supported by the National Science Foundation of the United  
288 States grant 1722969. The experiments were performed at GeoSoilEnviroCARS (Sector 13),  
289 Partnership for Extreme Crystallography program (PX<sup>2</sup>), Advanced Photon Source (APS), and  
290 Argonne National Laboratory. GeoSoilEnviroCARS is supported by the National Science  
291 Foundation—Earth Sciences (EAR-1128799) and Department of Energy—Geosciences (DE-  
292 FG02-94ER14466). PX<sup>2</sup> program is supported by COMPRES under NSF Cooperative  
293 Agreement EAR 11-57758. The use of the COMPRES-GSECARS gas loading system was  
294 supported by COMPRES under NSF Cooperative Agreement EAR 11-57758 and by GSECARS.  
295 Use of the Advanced Photon Source was supported by the U.S. Department of Energy, Office of  
296 Science, Office of Basic Energy Sciences, under Contract No. DE-AC02-06CH11357. Readers  
297 can access the additional data in the supporting information. We would like to thank two  
298 anonymous reviewers for their thorough and helpful comments, which help to improve the  
299 quality of this manuscript. We would like to thank Susannah Dorfman for handling this  
300 manuscript.

## 301 References

- 302 Andraut, D., Bouhifd, M., Itie, J., and Richet, P. (1995) Compression and amorphization of (Mg, Fe)<sub>2</sub>SiO<sub>4</sub> olivines:  
303 an X-ray diffraction study up to 70 GPa. *Physics and Chemistry of Minerals*, 22(2), 99-107.
- 304 Angel, R., Downs, R., and Finger, L. (2000) High-temperature-high-pressure diffractometry. *Reviews in*  
305 *Mineralogy and Geochemistry*, 41(1), 559-597.
- 306 Angel, R.J. (2000) Equations of state. *Reviews in Mineralogy and Geochemistry*, 41(1), 35-59.
- 307 Angel, R.J., Alvaro, M., and Nestola, F. (2018) 40 years of mineral elasticity: a critical review and a new  
308 parameterisation of equations of state for mantle olivines and diamond inclusions. *Physics and Chemistry*  
309 *of Minerals*, 45(2), 95-113.
- 310 Angel, R.J., Bujak, M., Zhao, J., Gatta, G.D., and Jacobsen, S.D. (2007) Effective hydrostatic limits of pressure  
311 media for high-pressure crystallographic studies. *Journal of Applied Crystallography*, 40(1), 26-32.
- 312 Angel, R.J., Gonzalez-Platas, J., and Alvaro, M. (2014) EosFit7c and a Fortran module (library) for equation of state  
313 calculations. *Zeitschrift Fur Kristallographie*, 229(5), 405-419.
- 314 Balan, E., Blanchard, M., Lazzeri, M., and Ingrin, J. (2017) Theoretical Raman spectrum and anharmonicity of  
315 tetrahedral OH defects in hydrous forsterite. *European Journal of Mineralogy*, 29(2), 201-212.
- 316 Balan, E., Ingrin, J., Delattre, S., Kovács, I., and Blanchard, M. (2011) Theoretical infrared spectrum of OH-defects  
317 in forsterite. *European Journal of Mineralogy*, 23(3), 285-292.
- 318 Bell, D.R., and Rossman, G.R. (1992) Water in Earth's mantle: The role of nominally anhydrous minerals. *Science*,  
319 255(5050), 1391-1397.
- 320 Bell, D.R., Rossman, G.R., Maldener, J., Endisch, D., and Rauch, F. (2003) Hydroxide in olivine: a quantitative  
321 determination of the absolute amount and calibration of the IR spectrum. *Journal of Geophysical Research:*  
322 *Solid Earth* (1978–2012), 108(B2).
- 323 Beran, A., and Libowitzky, E. (2006) Water in natural mantle minerals II: Olivine, garnet and accessory minerals.  
324 *Reviews in Mineralogy and Geochemistry*, 62(1), 169-191.
- 325 Berry, A.J., Hermann, J., O'Neill, H.S.C., and Foran, G.J. (2005) Fingerprinting the water site in mantle olivine.  
326 *Geology*, 33(11), 869-872.
- 327 Berry, A.J., O'Neill, H.S.C., Hermann, J., and Scott, D.R. (2007) The infrared signature of water associated with  
328 trivalent cations in olivine. *Earth and Planetary Science Letters*, 261(1-2), 134-142.
- 329 Birch, F. (1947) Finite elastic strain of cubic crystals. *Physical Review*, 71(11), 809-824.
- 330 -. (1978) Finite strain isotherm and velocities for single - crystal and polycrystalline NaCl at high pressures and 300  
331 K. *Journal of Geophysical Research: Solid Earth*, 83(B3), 1257-1268.
- 332 Chen, J., Liu, H., and Girard, J. (2011) Comparative in situ X-ray diffraction study of San Carlos olivine: Influence  
333 of water on the 410 km seismic velocity jump in Earth's mantle. *American Mineralogist*, 96(5-6), 697-702.
- 334 Dera, P., Zhuravlev, K., Prakapenka, V., Rivers, M.L., Finkelstein, G.J., Grubor-Urosevic, O., Tschauer, O., Clark,  
335 S.M., and Downs, R.T. (2013) High pressure single-crystal micro X-ray diffraction analysis with  
336 GSE\_ADA/RSV software. *High Pressure Research*, 33(3), 466-484.
- 337 Dolomanov, O.V., Bourhis, L.J., Gildea, R.J., Howard, J.A., and Puschmann, H. (2009) OLEX2: a complete  
338 structure solution, refinement and analysis program. *Journal of Applied Crystallography*, 42(2), 339-341.
- 339 Downs, R.T., Zha, C.-S., DuFFY, T.S., and Finger, L.W. (1996) The equation of state of forsterite to 17.2 GPa and  
340 effects of pressure media. *American Mineralogist*, 81(1-2), 51-55.
- 341 Dubrovinsky, L., Boffa-Ballaran, T., Glazyrin, K., Kurnosov, A., Frost, D., Merlini, M., Hanfland, M., Prakapenka,  
342 V., Schouwink, P., and Pippinger, T. (2010) Single-crystal X-ray diffraction at megabar pressures and  
343 temperatures of thousands of degrees. *High Pressure Research*, 30(4), 620-633.
- 344 Durben, D.J., McMillan, P.F., and Wolf, G.H. (1993) Raman study of the high-pressure behavior of forsterite  
345 (Mg<sub>2</sub>SiO<sub>4</sub>) crystal and glass. *American Mineralogist*, 78(11-12), 1143-1148.
- 346 Fan, D.W., Lu, C., Xu, J.G., Yan, B.M., Yang, B., and Chen, J.H. (2017) Effects of water on P-V-T equation of state  
347 of pyrope. *Physics of the Earth and Planetary Interiors*, 267, 9-18.
- 348 Fei, H.Z., Koizumi, S., Sakamoto, N., Hashiguchi, M., Yurimoto, H., Marquardt, K., Miyajima, N., and Katsura, T.  
349 (2018) Pressure, temperature, water content, and oxygen fugacity dependence of the Mg grain-boundary  
350 diffusion coefficient in forsterite. *American Mineralogist*, 103(9), 1354-1361.
- 351 Fei, Y., Ricolleau, A., Frank, M., Mibe, K., Shen, G., and Prakapenka, V. (2007) Toward an internally consistent  
352 pressure scale. *Proceedings of the National Academy of Sciences of the United States of America*, 104(22),  
353 9182-9186.

- Ferot, A., and Bolfan-Casanova, N. (2012) Water storage capacity in olivine and pyroxene to 14 GPa: Implications for the water content of the Earth's upper mantle and nature of seismic discontinuities. *Earth and Planetary Science Letters*, 349, 218-230.
- Finkelstein, G.J., Dera, P.K., Jahn, S., Oganov, A.R., Holl, C.M., Meng, Y., and Duffy, T.S. (2014) Phase transitions and equation of state of forsterite to 90 GPa from single-crystal X-ray diffraction and molecular modeling. *American Mineralogist*, 99(1), 35-43.
- Ghosh, S., Ohtani, E., Litasov, K.D., Suzuki, A., Dobson, D., and Funakoshi, K. (2013) Effect of water in depleted mantle on post-spinel transition and implication for 660km seismic discontinuity. *Earth and Planetary Science Letters*, 371, 103-111.
- Gonzalez-Platas, J., Alvaro, M., Nestola, F., and Angel, R. (2016) EosFit7-GUI: a new graphical user interface for equation of state calculations, analyses and teaching. *Journal of Applied Crystallography*, 49(4), 1377-1382.
- Hazen, R.M. (1976) Effects of temperature and pressure on the crystal structure of forsterite. *American Mineralogist*, 61(11-12), 1280-1293.
- Hushur, A., Manghnani, M.H., Smyth, J.R., Nestola, F., and Frost, D.J. (2009) Crystal chemistry of hydrous forsterite and its vibrational properties up to 41 GPa. *American Mineralogist*, 94(5-6), 751-760.
- Ita, J., and Stixrude, L. (1992) Petrology, elasticity, and composition of the mantle transition zone. *Journal of Geophysical Research*, 97(B5), 6849-6866.
- Jacobsen, S.D., Jiang, F., Mao, Z., Duffy, T.S., Smyth, J.R., Holl, C.M., and Frost, D.J. (2008) Effects of hydration on the elastic properties of olivine. *Geophysical Research Letters*, 35(14), L14303.
- Kohlstedt, D., Keppler, H., and Rubie, D. (1996) Solubility of water in the  $\alpha$ ,  $\beta$  and  $\gamma$  phases of  $(\text{Mg, Fe})_2\text{SiO}_4$ . *Contributions to Mineralogy and Petrology*, 123(4), 345-357.
- Kovács, I., O'Neill, H.S.C., Hermann, J.r., and Hauri, E.H. (2010) Site-specific infrared OH absorption coefficients for water substitution into olivine. *American Mineralogist*, 95(2-3), 292-299.
- Kudoh, Y., Kuribayashi, T., Kagi, H., and Inoue, T. (2006) Cation vacancy and possible hydrogen positions in hydrous forsterite,  $\text{Mg}_{1.985}\text{Si}_{1.0}\text{O}_{9.93}\text{H}_{0.06}\text{O}_4$ , synthesized at 13.5 GPa and 1300 C. *Journal of Mineralogical and Petrological Sciences*, 101(5), 265-269.
- Kudoh, Y., and Takéuchi, Y. (1985) The crystal structure of forsterite  $\text{Mg}_2\text{SiO}_4$  under high pressure up to 149 kb. *Zeitschrift für Kristallographie-Crystalline Materials*, 171(1-4), 291-302.
- Lemaire, C., Kohn, S., and Brooker, R. (2004) The effect of silica activity on the incorporation mechanisms of water in synthetic forsterite: a polarised infrared spectroscopic study. *Contributions to Mineralogy and Petrology*, 147(1), 48-57.
- Liu, L.-G. (1975) Disproportionation of  $\text{Ni}_2\text{SiO}_4$  to stishovite plus bunsenite at high pressures and temperatures. *Earth and Planetary Science Letters*, 24(3), 357-362.
- Liu, L.-G., and Mernagh, T. (1993) Raman spectra of forsterite and fayalite at high pressures and room temperature. *International Journal of High Pressure Research*, 11(5), 241-256.
- Manghnani, M.H., Hushur, A., Smyth, J.R., Nestola, F., Dera, P., Sekar, M., Amulele, G., and Frost, D.J. (2013) Compressibility and structural stability of two variably hydrated olivine samples ( $\text{Fo}_{97}\text{Fa}_3$ ) to 34 GPa by X-ray diffraction and Raman spectroscopy. *American Mineralogist*, 98(11-12), 1972-1979.
- Mao, H., Takahashi, T., and Bassett, W.A. (1970) Isothermal compression of the spinel phase of  $\text{Ni}_2\text{SiO}_4$  up to 300 kilobars at room temperature. *Physics of the Earth and Planetary Interiors*, 3, 51-53.
- Mao, Z., Jacobsen, S., Jiang, F., Smyth, J., Holl, C., Frost, D., and Duffy, T. (2010) Velocity crossover between hydrous and anhydrous forsterite at high pressures. *Earth and Planetary Science Letters*, 293(3-4), 250-258.
- Matveev, S., O'Neill, H.S.C., Ballhaus, C., Taylor, W.R., and Green, D. (2001) Effect of silica activity on  $\text{OH}^-$  IR spectra of olivine: implications for low- $\alpha\text{SiO}_2$  mantle metasomatism. *Journal of Petrology*, 42(4), 721-729.
- Momma, K., and Izumi, F. (2011) VESTA 3 for three-dimensional visualization of crystal, volumetric and morphology data. *Journal of Applied Crystallography*, 44(6), 1272-1276.
- Mosenfelder, J.L., Deligne, N.I., Asimow, P.D., and Rossman, G.R. (2006) Hydrogen incorporation in olivine from 2-12 GPa. *American Mineralogist*, 91(2-3), 285-294.
- Nestola, F., Pasqual, D., Smyth, J., Novella, D., Secco, L., Manghnani, M., and Negro, A.D. (2011) New accurate elastic parameters for the forsterite-fayalite solid solution. *American Mineralogist*, 96(11-12), 1742-1747.
- Nord, A.G., Annersten, H., and Filippidis, A. (1982) The cation distribution in synthetic Mg-Fe-Ni olivines. *American Mineralogist*, 67(11-12), 1206-1211.
- Novella, D., Bolfan-Casanova, N., Nestola, F., and Harris, J.W. (2015)  $\text{H}_2\text{O}$  in olivine and garnet inclusions still trapped in diamonds from the Siberian craton: Implications for the water content of cratonic lithosphere peridotites. *Lithos*, 230, 180-183.



- Pamato, M.G., Nestola, F., Novella, D., Smyth, J.R., Pasqual, D., Gatta, G.D., Alvaro, M., and Secco, L. (2019) The High-Pressure Structural Evolution of Olivine along the Forsterite–Fayalite Join. *Minerals*, 9(12), 790.
- Periotto, B., Balić-Žunić, T., Nestola, F., Katerinopoulou, A., and Angel, R.J. (2012) Re-investigation of the crystal structure of enstatite under high-pressure conditions. *American Mineralogist*, 97(10), 1741-1748.
- Peslier, A.H. (2010) A review of water contents of nominally anhydrous natural minerals in the mantles of Earth, Mars and the Moon. *Journal of Volcanology and Geothermal Research*, 197(1), 239-258.
- Peslier, A.H., Woodland, A.B., Bell, D.R., and Lazarov, M. (2010) Olivine water contents in the continental lithosphere and the longevity of cratons. *Nature*, 467(7311), 78-U108.
- Poe, B.T., Romano, C., Nestola, F., and Smyth, J.R. (2010) Electrical conductivity anisotropy of dry and hydrous olivine at 8 GPa. *Physics of the Earth and Planetary Interiors*, 181(3), 103-111.
- Qin, T., Wentzcovitch, R.M., Umemoto, K., Hirschmann, M.M., and Kohlstedt, D.L. (2018) Ab initio study of water speciation in forsterite: Importance of the entropic effect. *American Mineralogist*, 103(5), 692-699.
- Rauch, M., and Keppler, H. (2002) Water solubility in orthopyroxene. *Contributions to Mineralogy and Petrology*, 143(5), 525-536.
- Rivers, M., Prakapenka, V.B., Kubo, A., Pullins, C., Holl, C.M., and Jacobsen, S.D. (2008) The COMPRES/GSECARS gas-loading system for diamond anvil cells at the Advanced Photon Source. *High Pressure Research*, 28(3), 273-292.
- Rouquette, J., Kantor, I., McCammon, C., Dmitriev, V., and Dubrovinsky, L. (2008) High-pressure studies of (Mg<sub>0.9</sub>Fe<sub>0.1</sub>)<sub>2</sub>SiO<sub>4</sub> olivine using Raman spectroscopy, X-ray diffraction, and Mössbauer spectroscopy. *Inorganic Chemistry*, 47(7), 2668-2673.
- Sheldrick, G.M. (2008) A short history of SHELX. *Acta Crystallogr A*, 64(Pt 1), 112-22.
- Smyth, J.R., Frost, D.J., Nestola, F., Holl, C.M., and Bromiley, G. (2006) Olivine hydration in the deep upper mantle: Effects of temperature and silica activity. *Geophysical Research Letters*, 33(15).
- Tenner, T.J., Hirschmann, M.M., Withers, A.C., and Ardia, P. (2012) H<sub>2</sub>O storage capacity of olivine and low-Ca pyroxene from 10 to 13 GPa: consequences for dehydration melting above the transition zone. *Contributions to Mineralogy and Petrology*, 163(2), 297-316.
- Umemoto, K., Wentzcovitch, R.M., Hirschmann, M.M., Kohlstedt, D.L., and Withers, A.C. (2011) A first-principles investigation of hydrous defects and IR frequencies in forsterite: The case for Si vacancies. *American Mineralogist*, 96(10), 1475-1479.
- Walker, A.M., Hermann, J., Berry, A.J., and O'Neill, H.S.C. (2007) Three water sites in upper mantle olivine and the role of titanium in the water weakening mechanism. *Journal of Geophysical Research-Solid Earth*, 112(B5).
- Wang, L., Miyajima, N., Kawazoe, T., and Katsura, T. (2019) Activation of [100](001) slip system by water incorporation in olivine and the cause of seismic anisotropy decrease with depth in the asthenosphere. *American Mineralogist*, 104(1), 47-52.
- Will, G., Hoffbauer, W., Hinze, E., and Lauterjung, J. (1986) The compressibility of forsterite up to 300 kbar measured with synchrotron radiation. *Physica B+C*, 139, 193-197.
- Xu, J., Zhang, D., Dera, P., Zhang, B., and Fan, D. (2017a) Experimental evidence for the survival of augite to transition zone depths, and implications for subduction zone dynamics. *American Mineralogist*, 102(7), 1516-1524.
- Xu, J., Zhang, D., Fan, D., Downs, R.T., Hu, Y., and Dera, P. (2017b) Isosymmetric pressure-induced bonding increase changes compression behavior of clinopyroxenes across jadeite-aegirine solid solution in subduction zones. *Journal of Geophysical Research: Solid Earth*, 122(1), 142-157.
- Xu, J., Zhang, D., Fan, D., Zhang, J.S., Hu, Y., Guo, X., Dera, P., and Zhou, W. (2018) Phase Transitions in Orthoenstatite and Subduction Zone Dynamics: Effects of Water and Transition Metal Ions. *Journal of Geophysical Research: Solid Earth*, 123(4), 2723-2737.
- Xue, X., Kanzaki, M., Turner, D., and Lorocho, D. (2017) Hydrogen incorporation mechanisms in forsterite: New insights from 1H and 29Si NMR spectroscopy and first-principles calculation. *American Mineralogist*, 102(3), 519-536.
- Yang, Y., Liu, W., Qi, Z., Wang, Z., Smyth, J.R., and Xia, Q. (2019) Re-configuration and interaction of hydrogen sites in olivine at high temperature and high pressure. *American Mineralogist*, 104(6), 878-889.
- Zha, C.-S., Duffy, T.S., Downs, R.T., Mao, H.-K., and Hemley, R.J. (1998) Brillouin scattering and X-ray diffraction of San Carlos olivine: direct pressure determination to 32 GPa. *Earth and Planetary Science Letters*, 159(1), 25-33.
- Zha, C.-S., Duffy, T.S., Downs, R.T., Mao, H.K., and Hemley, R.J. (1996) Sound velocity and elasticity of single - crystal forsterite to 16 GPa. *Journal of Geophysical Research*, 101(B8), 17535-17545.

- 466 Zhang, D., Dera, P.K., Eng, P.J., Stubbs, J.E., Zhang, J.S., Prakapenka, V.B., and Rivers, M.L. (2017a) High  
467 Pressure Single Crystal Diffraction at PX<sup>2</sup>. Journal of visualized experiments: JoVE(119), e54660.  
468 Zhang, D., Hu, Y., Xu, J., Downs, R.T., Hammer, J.E., and Dera, P.K. (2019) High-pressure behavior of  
469 liebenbergite: The most incompressible olivine-structured silicate. American Mineralogist, 104(4), 580-  
470 587.  
471 Zhang, J.S., Hu, Y., Shelton, H., Kung, J., and Dera, P. (2017b) Single-crystal X-ray diffraction study of Fe<sub>2</sub>SiO<sub>4</sub>  
472 fayalite up to 31 GPa. Physics and Chemistry of Minerals, 44(3), 171-179.  
473 Zhang, L. (1998) Single crystal hydrostatic compression of (Mg, Mn, Fe, Co)<sub>2</sub>SiO<sub>4</sub> olivines. Physics and chemistry  
474 of minerals, 25(4), 308-312.  
475 Zhang, L., Ahsbahs, H., Hafner, S.S., and Kutoglu, A. (1997) Single-crystal compression and crystal structure of  
476 clinopyroxene up to 10 GPa. American Mineralogist, 82(3), 245-258.  
477

478

## 479 **Figures**

480 **Figure 1.** Selected unpolarized FTIR spectra of hydrous olivine synthesized at 4 GPa and 1250  
 481 °C. Integration of the spectrum indicates an H<sub>2</sub>O content of 1538 ppmw.

482 **Figure 2.** Single crystal X-ray diffraction patterns of hydrous olivine at (a).  $P = 1.2(1)$  GPa and  
 483 (b)  $P = 29.9(2)$  GPa.

484 **Figure 3.** Evolution of unit-cell parameters as a function of pressure for the hydrous olivine in  
 485 this study: (a)  $a$ , (b)  $b$ , (c)  $c$ , and (d)  $V$ . Mg-rich ( $\text{Fo} \geq 95$ ) olivine from previous studies are  
 486 also shown for comparison (Hazen 1976; Kudoh and Takéuchi 1985; Will et al. 1986;  
 487 Downs et al. 1996; Zhang 1998; Poe et al. 2010; Manghnani et al. 2013; Finkelstein et al.  
 488 2014; Pamato et al. 2019). Solid lines correspond to the BM3 EoS of this study.

489 **Figure 4.** Eulerian strain-normalized pressure ( $F_E$ - $f_E$ ) plot (Angel 2000) ( $F_E = P/3f_E (1 + 2f_E)^{5/2}$ ;  
 490  $f_E = [(V_0/V)^{2/3} - 1]/2$ ) of  $a$  (a)  $b$  (b),  $c$  (c), and  $V$  (d) for the hydrous olivine in this study.

491 **Figure 5.** Normalized polyhedral volume as a function of a normalized unit-cell volume at  
 492 different pressures. The solid line represents the  $y = x$  line. The error bars were calculated  
 493 using the method described by Zhang et al. (2019).

494 **Figure 6.** Pressure dependence of M1-O bond lengths for the hydrous olivine in this study: (a)  
 495 M1-O1, (b) M1-O2, (c) M1-O3 and (d) M1-O average. Mg-rich ( $\text{Fo} \geq 95$ ) olivine from  
 496 previous studies are also shown for comparison (Hazen 1976; Kudoh and Takéuchi 1985;  
 497 Pamato et al. 2019). The solid lines represent weighted linear regression results (Table S8)  
 498 for the data of Pamato et al. (2019) (red lines) and this study (black lines).

499 **Figure 7.** Pressure dependence of M2-O bond lengths for the hydrous olivine in this study: (a)  
 500 M2-O1, (b) M2-O2, (c) M2-O3a and M2-O3b, and (d) M2-O average. Mg-rich ( $\text{Fo} \geq 95$ )

olivine from previous studies are also shown for comparison (Hazen 1976; Kudoh and Takéuchi 1985; Pamato et al. 2019). The solid lines represent weighted linear regression results (Table S8) for the data of Pamato et al. (2019) (red lines) and this study (black lines)

**Figure 8.** Pressure dependence of Si-O bond lengths for the hydrous olivine in this study: (a) Si-O1, (b) Si-O2, (c) Si-O3 and (d) Si-O average. Mg-rich ( $Fo \geq 95$ ) olivine from previous studies are also shown for comparison (Hazen 1976; Kudoh and Takéuchi 1985; Pamato et al. 2019). The solid lines represent weighted linear regression results (Table S8) for the data of Pamato et al. (2019) (red lines) and this study (black lines)

**Figure 9.** Pressure dependence of polyhedral volumes for the hydrous olivine in this study: (a)  $M1O_6$ , (b)  $M2O_6$  and (c)  $SiO_4$ . Mg-rich ( $Fo \geq 95$ ) olivine from the previous study is also shown for comparison (Pamato et al. 2019). The solid lines represent weighted linear regression results (Table S8) for the data of Pamato et al. (2019) (red lines) and this study (black lines)

Figure 1

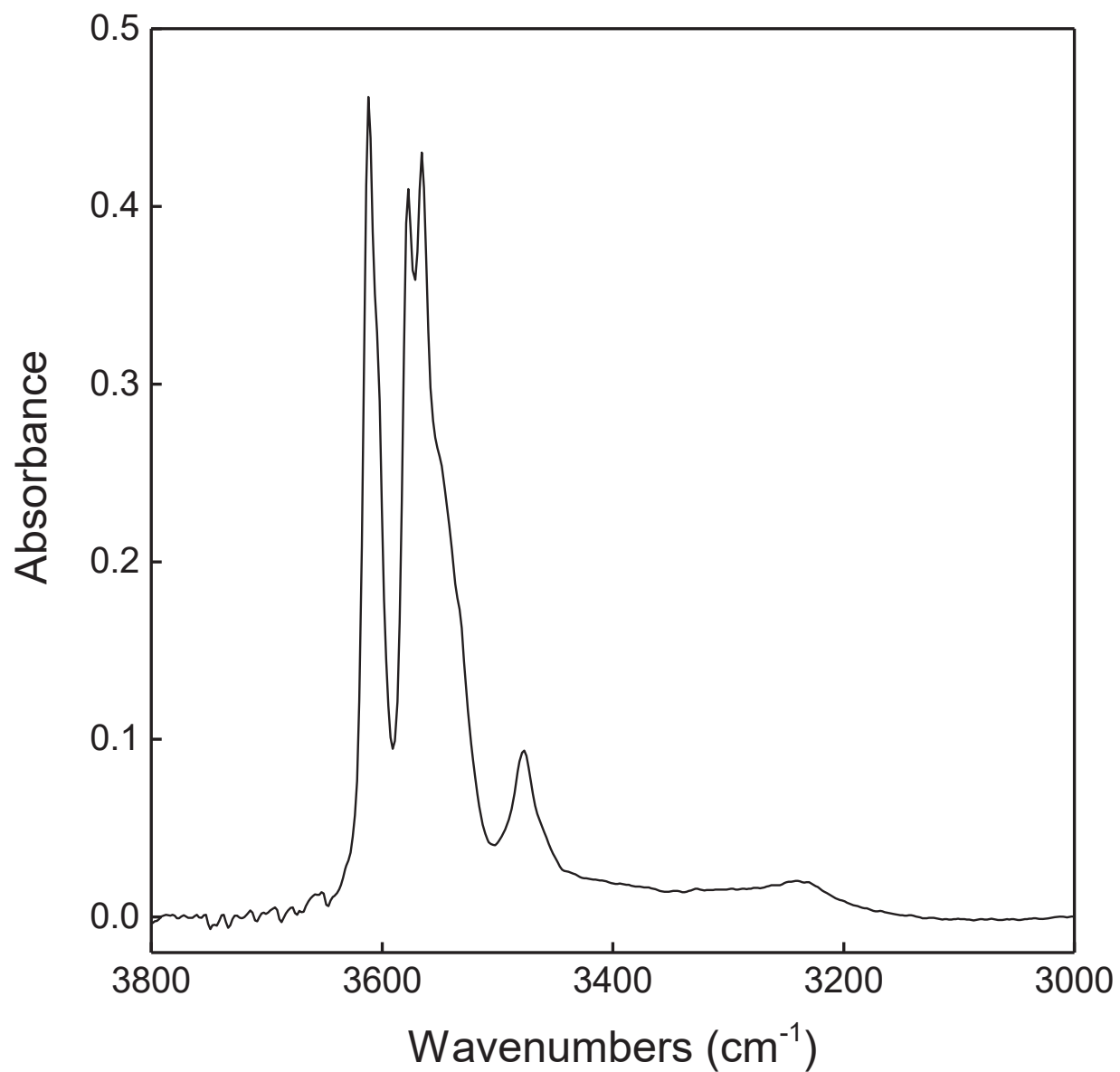


Figure 2

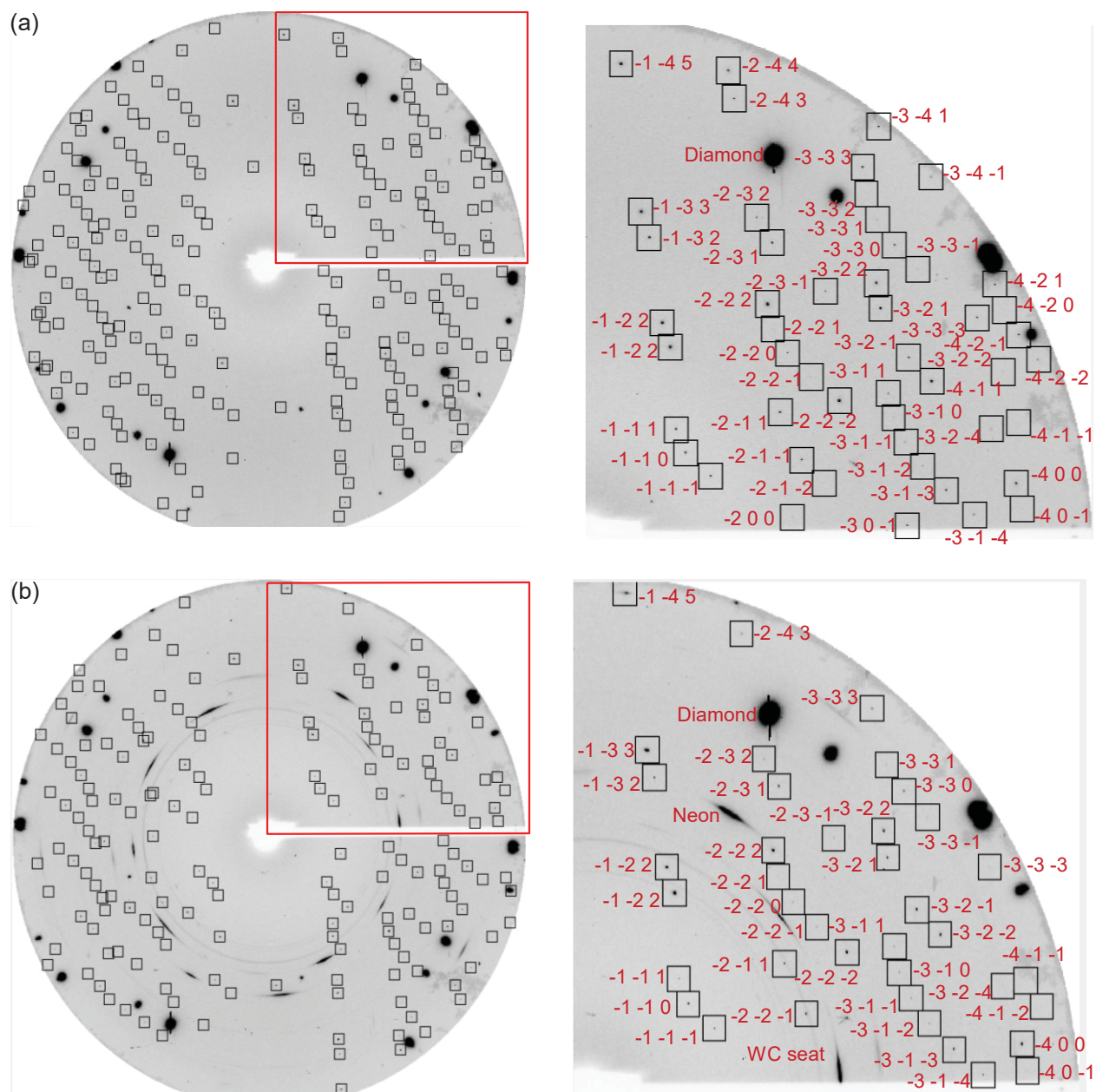


Figure 3

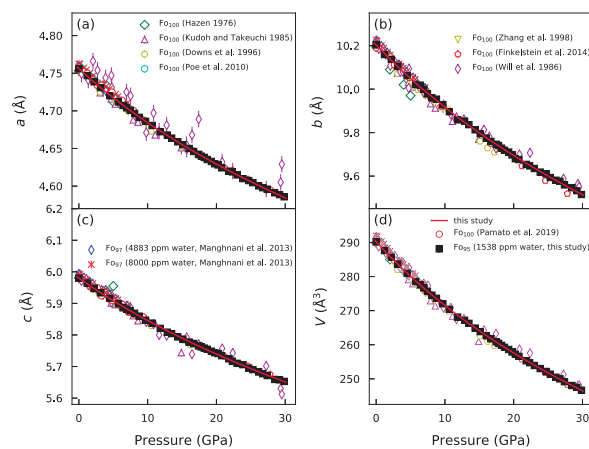


Figure 4

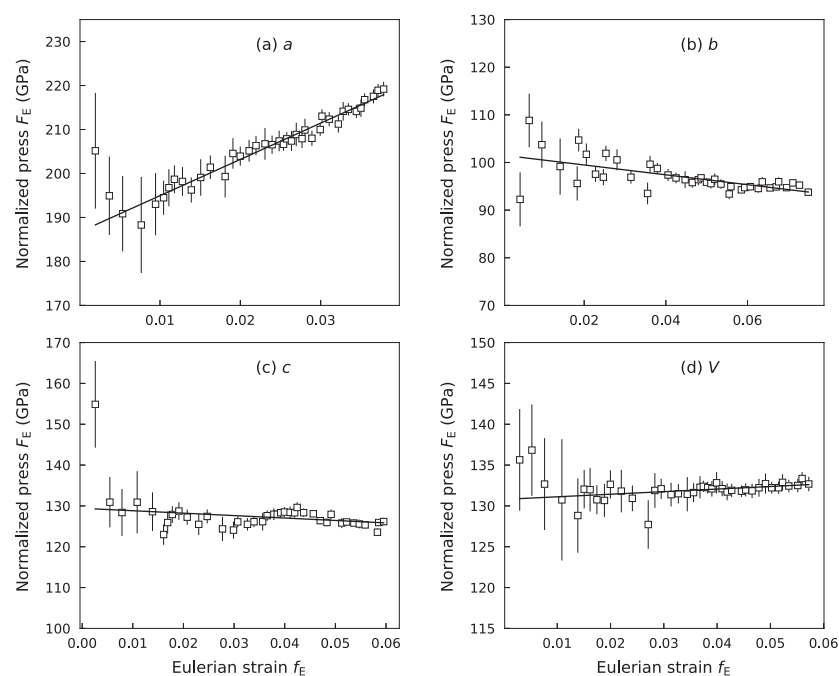




Figure 5

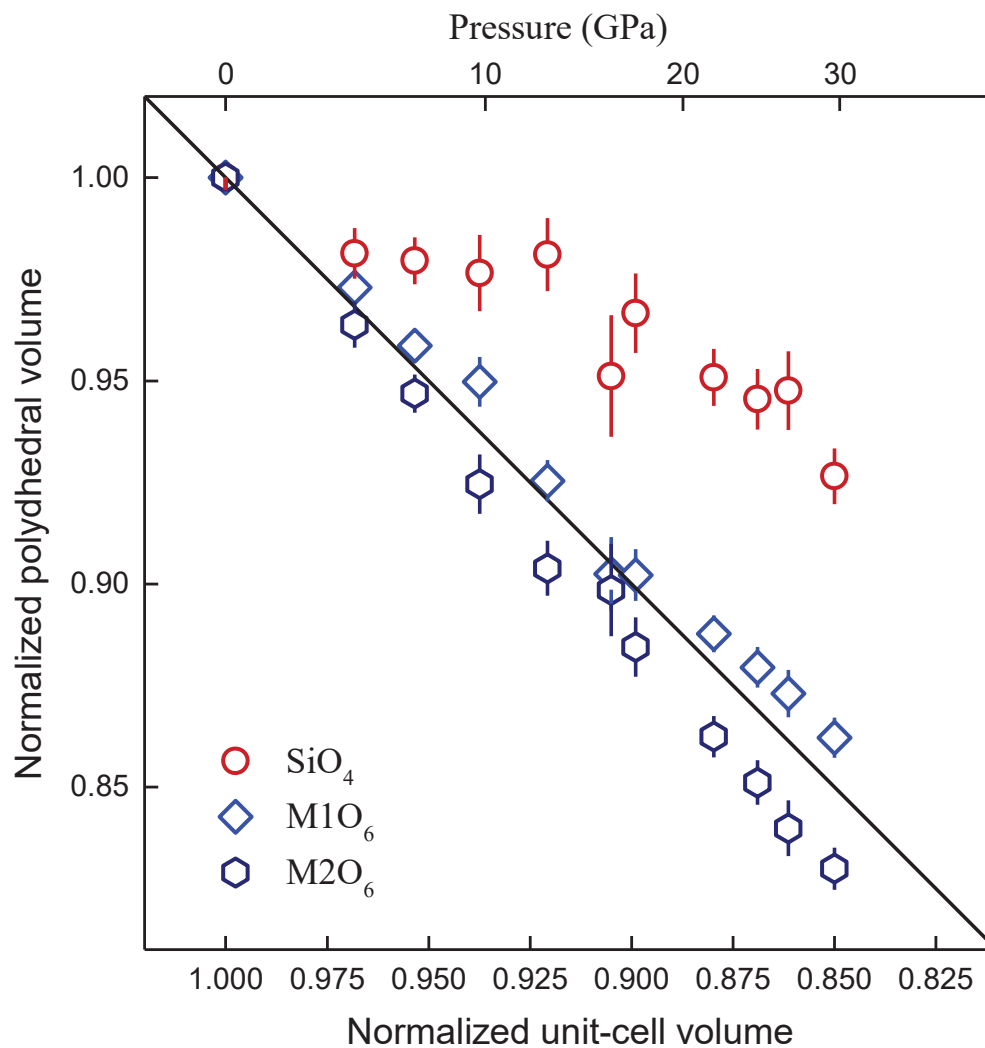


Figure 6

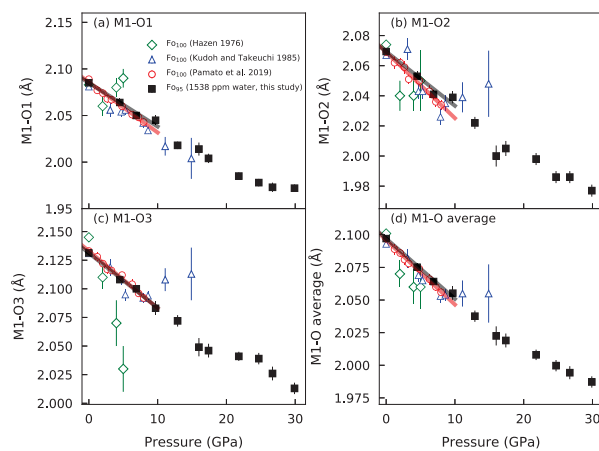


Figure 7

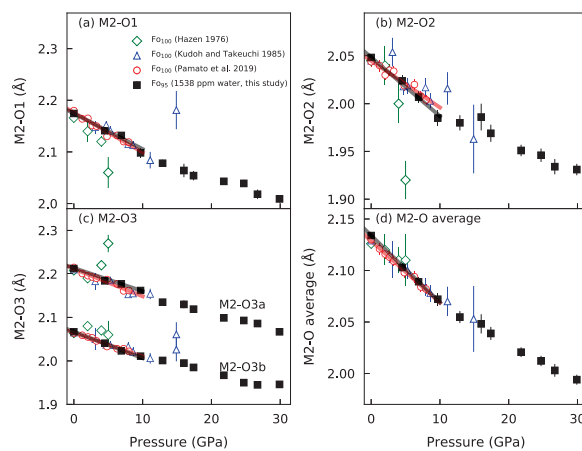


Figure 8

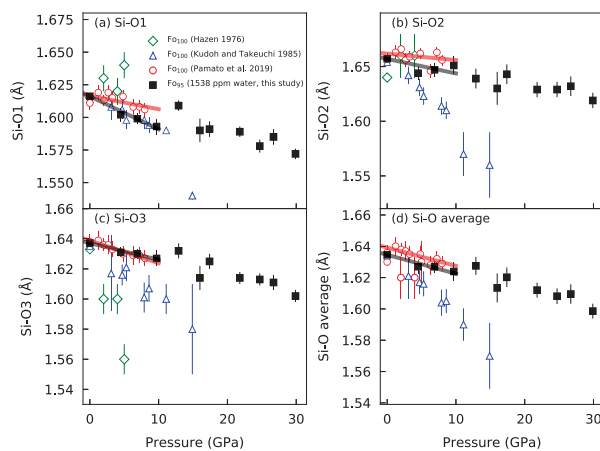


Figure 9

